Received: 8 September 2017 | Revised: 15 January 2018 | Accepted: 18 January 2018

DOI: 10.1111/pce.13205

ORIGINAL ARTICLE

WILEY Plant, Cell & Environment

Water relations of *Calycanthus* flowers: Hydraulic conductance, capacitance, and embolism resistance

Adam B. Roddy[1,2] | Kevin A. Simonin[3] | Katherine A. McCulloh[4] | Craig R. Brodersen[2] | Todd E. Dawson[1]

[1] Department of Integrative Biology, University of California-Berkeley, Berkeley, CA 94720, USA

[2] School of Forestry and Environmental Studies, Yale University, New Haven, CT 06511, USA

[3] Department of Biology, San Francisco State University, San Francisco, CA 94132, USA

[4] Department of Botany, University of Wisconsin-Madison, Madison, WI 53706, USA

Correspondence
A. B. Roddy, School of Forestry and Environmental Studies, Yale University, New Haven, CT 06511, USA.
Email: adam.roddy@yale.edu

Funding information
U.S. Department of Energy, Grant/Award Number: DE-AC01-05CH11231; U.S. National Science Foundation; Yale Institute for Biospheric Studies

Abstract

For most angiosperms, producing and maintaining flowers is critical to sexual reproduction, yet little is known about the physiological processes involved in maintaining flowers throughout anthesis. Among extant species, flowers of the genus *Calycanthus* have the highest hydraulic conductance and vein densities of species measured to date, yet they can wilt by late morning under hot conditions. Here, we combine diurnal measurements of gas exchange and water potential, pressure–volume relations, functional responses of gas exchange, and characterization of embolism formation using high resolution X-ray computed microtomography to determine drought responses of *Calycanthus* flowers. Transpiration from flowers frequently exceeded transpiration from leaves, and flowers were unable to limit transpiration under conditions of high vapour pressure deficit. As a result, they rely heavily on hydraulic capacitance to prevent water potential declines. Despite having high water potentials at turgor loss, flowers were very resistant to embolism formation, with no embolism apparent until tepal water potentials had declined to −2 MPa. Although *Calycanthus* flowers remain connected to the stem xylem and have high hydraulic capacitance, their inability to curtail transpiration leads to turgor loss. These results suggest that extreme climate events may cause flower failure, potentially preventing successful reproduction.

KEYWORDS

Calycanthus, embolism, flower, hydraulic conductance, microCT, water balance

1 | INTRODUCTION

Flowers are developmentally and morphologically complex structures whose primary function is to promote sexual reproduction (Specht & Bartlett, 2009). Coevolution with animal pollinators has long been considered the primary selective agent responsible for the many diverse forms apparent among angiosperm flowers (Fenster, Armbruster, Wilson, Dudash, & Thomson, 2004; Sprengel, 1793, 1996). Yet floral adaptations to attract pollinators may not be as ubiquitous as commonly considered, and nonpollinator agents of selection, such as the resource costs of building and maintaining flowers, may also influence floral form and function (Herrera, 1996; Strauss & Whittall, 2006). For example, the water costs of flowers can limit flower size and impede leaf function (Galen, 1999; Galen, Sherry, & Carroll, 1999; Lambrecht, 2013; Lambrecht & Dawson, 2007; Teixido & Valladares, 2013, 2014). This requirement of maintaining water balance has led to coordinated shifts in hydraulic traits that vary systematically across the angiosperm phylogeny (Roddy, Brodersen, & Dawson, 2016) and with other pollination traits, such as floral lifespan (Zhang et al., 2017).

The resource investment required to produce and maintain flowers, as well as how and when these resources are allocated, can be highly variable among species and habitats (Bazzaz, Chiariello, Coley, & Pitelka, 1987; Reekie & Bazzaz, 1987a, 1987b; Roddy et al.,

2016; Teixido & Valladares, 2014). This variation could be due to a number of causes, including environmental conditions and differences in the functions performed by flowers (e.g., attracting pollinators or protecting the developing embryo; Galen, Dawson, & Stanton, 1993; Lambrecht & Dawson, 2007; Roddy & Dawson, 2012). For example, higher temperatures, increased evaporative demand, and nectar secretion can all lead to higher carbon and water requirements for some flowers (De la Barrera & Nobel, 2004; Patiño & Grace, 2002; Patiño, Jeffree, & Grace, 2002). Furthermore, underlying this diversity in construction and maintenance costs may also be a fundamental shift early in angiosperm evolution in the mechanisms of water import to flowers. For example, early-divergent *Illicium* and *Magnolia* flowers are hydrated predominantly by the xylem (Feild, Chatelet, & Brodribb, 2009a, 2009b) whereas some eudicot flowers are hypothesized to be hydrated by the phloem (Chapotin, Holbrook, Morse, & Gutiérrez, 2003; Trolinder, McMichael, & Upchurch, 1993). Large variation in whole flower hydraulic conductance (K_{flower}; Roddy et al., 2016) and in the pathways of water import suggest that, unlike angiosperm leaves, which rely predominantly on high fluxes of water transport to maintain turgor and gas exchange (Simonin & Roddy, 2018), flowers may use a variety of mechanisms to maintain turgor and remain functional during anthesis.

Whether the mechanisms of maintaining turgor in flowers represent more extreme versions of those employed by leaves or are fundamentally different is still unclear. Like leaves, water may be continuously supplied by the xylem, which would come with the risk of drought-induced embolism formation and spread (Zhang & Brodribb, 2017). Yet others have suggested that the phloem may serve as the primary source of water (Chapotin et al., 2003). Additionally, flowers may also rely primarily on water imported early in development, which is then slowly depleted throughout anthesis with some continuous supply by either the xylem or the phloem. Consistent with this, flowers have high hydraulic capacitance (Chapotin et al., 2003), which can buffer water potential declines and help to physiologically isolate flower water status from changes in the water status of the rest of the plant or from changes in atmospheric conditions. Flowers undoubtedly employ some combination of all these strategies, and there may be trade-offs between these strategies, as there are in stems and in leaves (Brodribb, Holbrook, Zwieniecki, & Palma, 2005; McCulloh, Johnson, Meinzer, & Woodruff, 2014; Meinzer, Johnson, Lachenbruch, McCulloh, & Woodruff, 2009).

In previous studies of K_{flower} and other hydraulic traits (Roddy et al., 2013; Roddy, Brodersen, & Dawson, 2016), flowers of the genus *Calycanthus* (Calycanthaceae; Zhou, Renner, & Wen, 2006) consistently had traits associated with high rates of water supply via the xylem (i.e., high vein length per area), high water loss (minimum epidermal conductance; g_{min}), and high hydraulic conductance (K_{flower}). These extreme trait values, particularly for *Calycanthus occidentalis*, suggest that these flowers can transport substantial amounts of water, possibly even outpacing leaf transpiration. Yet during hot, dry conditions *Calycanthus* flowers readily wilt by midday, suggesting that high hydraulic conductance and vein density are incapable of preventing turgor loss and, possibly, hydraulic failure. Using leaves as a comparison, we characterized the diurnal patterns of gas exchange and water potential, pressure–volume relations, and vulnerability to embolism of *Calycanthus* flowers to determine the relationships and trade-offs between these different mechanisms for maintaining floral hydraulic function. We focused our measurements on *C. occidentalis*, native to California, but include data for the other two species in the genus: *Calycanthus floridus*, native to the southeastern United States; and *Calycanthus chinensis*, native to China.

2 | MATERIALS AND METHODS

2.1 | Plant species, study site, and microclimate measurements

Between May 5 and 25, 2014, we studied three individuals of each of *C. occidentalis* and *C. chinensis* growing at the University of California Botanical Garden with additional measurements made in 2015 and 2016. These data were supplemented with data collected in 2015–2017 from *C. floridus* growing in the U.C. Botanical Garden and in the Marsh Botanic Garden, New Haven, CT. All statistical analyses were performed using R (v. 3.4.3; R Core Team, 2017).

C. occidentalis and *C. chinensis* were watered twice weekly throughout the study. The three *C. chinensis* individuals were growing in a more shaded microsite than the three *C. occidentalis* individuals. We characterized microclimate and calculated vapour pressure deficit (VPD) of the atmosphere as (Buck, 1981):

$$VPD = \left(0.61121 * e^{\frac{17.502 * T_a}{T_a + 240.97}}\right)\left(1 - \frac{RH}{100}\right),$$

where T_a and RH are air temperature (°C) and relative humidity (%), respectively. T_a and RH measurements were recorded every 5 min with Hobo U23 (Onset Corp., Bourne, MA) data loggers that were housed in a covered, white, PVC T-shaped tube and hung 2 m off the ground within 100 m of both species.

At the U.C. Botanical Garden, anthesis begins in May for *C. occidentalis* and *C. chinensis* and lasts into June with fewer flowers towards the end of this period. Throughout the flowering period, flowers of all stages of development are present. Flowers of *C. occidentalis* and *C. floridus* are composed of a variable number of graded tepals, whereas those of *C. chinensis* have a variable number of tepals that are of two, more distinctive morphologies. Tepals tend to wilt and senesce starting at the tip moving towards the tepal base during anthesis. For all measurements, we sampled only newly opened flowers less than a day into anthesis. Each flower lasts for a few days, during which time they are entered by and provide shelter for venturous beetles (Grant, 1950).

2.2 | Diurnal measurements of gas exchange and water potential

We measured water vapour flux from entire flowers and parts of leaves of both species using an infrared gas analyser equipped with a clear chamber (LI 6400 outfitted with the LI 6400-05 conifer chamber, LI-COR Biosciences, Lincoln, NE). With this chamber, leaf and

flower temperatures were calculated based on energy balance, and the light level was not controlled. All measurements were made under ambient humidity, and the reference CO_2 concentration was set to 400 ppm. At each time period on each plant, we measured at least one newly opened flower and, separately, a subtending leaf. We waited until fluxes had stabilized before recording five instantaneous measurements over approximately 10 s and subsequently averaging these. On May 5, 2014, we measured gas exchange and water potentials of *C. occidentalis* at predawn (4:00–6:00 a.m.) and every 3 hr after dawn (8:30 a.m., 11:30 a.m., 2:30 p.m., 5:30 p.m.) and *C. chinensis* individuals at only predawn and midday (2:30 p.m.). Based on these data, the lowest daily water potentials and highest gas exchange rates occurred at midday (2:30 p.m.). Therefore, for subsequent measurements, we chose to sample only at predawn and midday and to sample multiple flowers per plant at these two time periods. In May 2015, predawn and midday water potentials of flowers, leaves, and stems were sampled again to supplement and corroborate measurements from 2014. Similarly, stem, leaf, and flower water potentials of *C. floridus* growing in New Haven, CT, were measured in 2015 and 2016 to confirm they followed a similar diurnal pattern.

On the evening prior to gas exchange measurements, we covered one leaf subtending each flower in plastic wrap and aluminum foil so that this leaf could be used to estimate stem water potential on the subsequent day. Immediately after gas exchange measurements, the measured leaf and flower were wrapped in plastic wrap and excised with the adjacent foiled leaf and placed into a humidified plastic bag kept in a cool box and allowed to equilibrate for approximately 30 min. The balancing pressure was measured using a Scholander-style pressure chamber (SAPS, Soil Moisture Equipment Corp., Santa Barbara, CA, USA) with a resolution of 0.02 MPa. While inside the pressure chamber, leaves were kept covered by plastic wrap or plastic wrap and foil and flowers were wrapped in a plastic bag to prevent, as best as possible, desiccation inside the chamber during measurement. After water potential measurements, we transported the leaves and flowers to the lab and used a flatbed scanner and ImageJ (v. 1.47v) to estimate their surface areas, which were then used to recalculate gas exchange rates. Predawn gas exchange measurements for *C. occidentalis* leaves on May 5 are not included, however, because these leaves were misplaced before their areas could be measured.

From gas exchange and water potential measurements, we calculated flower and leaf hydraulic conductance based on Darcy's law (Whitehead, 1998):

$$K = \frac{E}{\Delta\Psi},$$

where K is the hydraulic conductance (mmol m^{-2} s^{-1} MPa^{-1}), E is the transpiration rate (mmol m^{-2} s^{-1}), and $\Delta\Psi$ is the difference between stem and leaf or between stem and flower water potentials ($\Delta\Psi_{stem-leaf}$ or $\Delta\Psi_{stem-flower}$). This method assumes an approximate mass balance between the fluxes of liquid water into the structure (driven by $\Delta\Psi$) and water vapour loss from the structure (E). Given the large water contents and slow water turnover times of flowers, this assumption was likely violated during times of low transpiration, such as during the early morning and evening.

2.3 | Pressure–volume analysis

We determined the relationship between Ψ and relative water content (RWC) of four to five whole flowers and leaves per species using repeated measures of mass and Ψ (Tyree & Hammel, 1972). For each species, shoots with leaves and flowers were collected between 7:30–8:30 a.m. on cloudy days. Shoots approximately 1 m in length were cut from the plant and immediately recut by at least 10 cm one to two times underwater. Cut ends were kept in water during transportation back to the lab, and until specimens were excised for measurements. From each shoot, one leaf and one flower were chosen for pressure–volume measurements. Repeated measurements of mass and water potential were made as samples slowly desiccated to construct the relationship between water content and water potential (i.e., pressure–volume curves). Mass was recorded immediately before and after each water potential measurement and subsequently averaged, and 10–12 measurements were made on each specimen. Specimens were then oven-dried at 60 °C for a week to determine dry mass. From these pressure–volume curves, we determined the Ψ and RWC at the turgor loss point (Ψ_{TLP} and RWC_{TLP}) by a regression through at least five points of the linear part of the curve, the saturated water content per dry weight (g g^{-1}) from the linear extrapolation to the x-intercept of the Ψ versus water mass relationship normalized to dry mass, the modulus of elasticity from the slope of the relationship between turgor pressure and RWC above the turgor loss point, capacitance (MPa^{-1}) and absolute capacitance (mol H_2O kg^{-1} dry mass MPa^{-1}) from the slope of the relationship between RWC and Ψ above the turgor loss point, and the saturated water content. Parameters were calculated using standard major axis regressions, and differences in calculated parameters between structures and species were analysed using R. To test whether midday water potential declines are linked with hydraulic capacitance, we pooled data for species and structures and used standardized major axis regression to account for variance in both axes (the "sma" function in the package *smatr*).

Stem hydraulic capacitance was calculated from water release curves of small chunks of small diameter (~1 cm) branches following previously published methods (McCulloh et al., 2014). Three shoots per species were sampled and five samples per species were used in the measurements. Samples were collected in the early morning, wrapped in wet paper towels, and kept refrigerated until analysis. All samples were vacuum infiltrated overnight in water. Excess water was removed from the samples by blotting them with paper towels, after which they were weighed and placed in screen cage thermocouple psychrometer chambers (83 series; JRD Merrill Specialty Equipment, Logan, UT, USA). Chambers were then triple-bagged and submerged in a cooler of water for 2–3 hr to allow equilibration between the sample and the chamber air under isothermal conditions. After equilibration, millivolt readings were recorded using a psychrometer reader (Psypro; Wescor, Logan, UT, USA). Samples were then removed from the chambers, weighed, and allowed to dry on the bench top for approximately 30 min before being returned to the

chambers to repeat the measurements. The mV readings from the psychrometer reader were converted to MPa based on calibration curves from salt solutions of known water potentials (Brown & Bartos, 1982). Samples were measured repeatedly until water potential values reached approximately −4 MPa, below which the psychrometers could not reliably resolve water potentials. Samples were oven-dried at 60 °C for at least 3 days before weighing the dry mass. *RWC* was calculated for each measurement and converted to relative water deficit as 1−*RWC*. The product of relative water deficit and the mass of water per unit tissue volume at saturation (M_w) yielded the cumulative mass of the water lost for each measurement interval. M_w was calculated as:

$$M_w = \left(\frac{M_s}{M_d}\rho\right) - \rho,$$

where ρ is wood density and M_s and M_d are the saturated and dry masses of the sample, respectively. The initial, linear phase of the plot of cumulative mass of water lost versus sapwood water potential gave the capacitance over the likely in situ physiological operating range of stem water potential (Meinzer et al., 2008; Meinzer, James, Goldstein, & Woodruff, 2003). This regression of the initial linear phase was forced through the origin because of the physical impossibility of water being released at 0 MPa. How many of these initial points were used was similar to the method commonly used for analysing pressure–volume curves of leaves. In this case, −1/Ψ was plotted against the amount of water released, and the number of initial points of this curve determined by adding points until the coefficient of variation declined. Stem hydraulic capacitance was calculated as the slope of the regression between the origin and this final point on the plot of Ψ versus water released. Based on wood volume and density, hydraulic capacitance could be expressed in the same units as it is expressed for leaves and stems (mol H_2O kg^{-1} dry mass MPa^{-1}).

2.4 | Water loss rates and residence times

At 11:45 a.m. on May 11, we excised three leaves and flowers per species to determine water loss rates. Cut surfaces were covered in petroleum jelly, and samples were weighed approximately every 15 min on an electronic balance. Between measurements, samples were kept out of direct sunlight but not protected from ambient wind. Flowers had visibly wilted but not substantially shrunken within about 1 hr after excision, at which point specimens were scanned to determine surface area, and water loss rates were expressed as mmol m^{-2} s^{-1}. Water loss rates measured in this way are a combination of stomatal and cuticular conductances. After excision and as tissue water potential declines, stomatal closure would reduce the relative contribution of stomatal conductance to overall water loss rates. To determine the effects of species and structure (flower vs. leaf) on water loss rates, we used a repeated measures analysis of variance with species and structure within time as the error term.

Water residence times were calculated from measurements of gas exchange and water potential as

$$\tau = \frac{W}{E},$$

where W is the leaf or flower water concentration per area (mol m^{-2}) and E is the transpiration rate (mmol m^{-2} s^{-1}). Because water content was not measured diurnally on the same samples measured for gas exchange, we estimated W from pressure–volume curves as the product of the RWC, the saturated water content (g g^{-1}), and the mass per area (g m^{-2}). Measurements of mass per area for flowers were made solely on tepals, whereas pressure–volume parameters were calculated from entire flowers (tepals, pedicel, and receptacle), which makes our estimates of W for flowers lower than they may actually be. The relationship between W and Ψ derived from pressure–volume measurements (Figure S1) was used to estimate W based on diurnal measurements of Ψ. Two-phase linear relationships were used for the extrapolations, where different linear functions were fit to the relationship between W and Ψ above and below the mean turgor loss points.

2.5 | Stomatal responses to VPD

Steady-state stomatal responses of *C. occidentalis* flowers and leaves to VPD were determined using a Walz GFS-3000 gas exchange system (Heinz Walz GmbH, Effeltrich, Germany). Flowering shoots were excised underwater in the morning, immediately recut underwater, and the cut end of the shoot kept in water during measurements. Individual tepals or leaves were enclosed in the cuvette. Starting at approximately 0.7 kPa, VPD was increased in steps of approximately 0.3 kPa up to approximately 2.5 kPa by changing humidity and flow rate. Across this range of VPD, g_s declined to below 50% of its maximum for each structure. After each step change in VPD, g_s was allowed to stabilize. Immediately after gas exchange measurements, the tissue enclosed in the cuvette was photographed, and its area later measured using ImageJ to recalculate gas exchange rates. Data were compiled for replicates and non-linear curves fit and compared to linear curves using the Akaike Information Criterion, with Akaike Information Criterion greater than five taken as indicative of a significantly better fit.

2.6 | Characterizing embolism formation

In a separate experiment, we quantified the water potential at which embolism appeared in tepals using high resolution X-ray computed microtomography (microCT; Brodersen & Roddy, 2016). In March 2015, flowering shoots of *C. floridus* were cut from plants growing at the U.C. Botanical Garden, recut underwater, and transported to the laboratory, where they were removed from water and allowed to slowly desiccate. Periodically, whole flowers were excised at the pedicel base and affixed in a custom, styrofoam holder that held one to two tepals in place. During microCT imaging, the entire flower was draped in a moist towel to minimize desiccation during the scan. The target tepals were imaged using continuous tomography at 24 keV while the sample was rotated from 0 to 180°. The duration of each scan was approximately 10 min, after which there was no visible damage to the tepals. Images were captured by a camera (PCO EDGE; Cooke Corp., Romulus, MI, USA) with a 5× magnification Mitutoyo long working distance lens. Scans resulted in 1,025 raw, two-dimensional projection images per sample, which were then reconstructed

into tomographic slices using an Octopus Software (Institute for Nuclear Science, University of Ghent, Belgium) plugin for ImageJ (Ruedin et al., 2017) and visualized in two dimensions in ImageJ and in three dimensions using Avizo 9 software package (FEI, Houston, TX, USA). Immediately after microCT imaging of the samples, the scanned regions of the tepals were excised and placed into thermocouple psychrometer chambers (83 series; JRD Merrill Specialty Equipment, Logan, UT, USA), which were then triple-bagged and placed into a 25 °C water bath for approximately 4 hr, and the water potentials assessed as above. Scoring presence/absence of embolism in tepals was done visually by examining the tomographic slices for the presence of continuous air embolisms in veins. Logistic regression was used to calculate as a function of water potential the 50% probability of there being any embolism present, using the functions "glm" and "dose.p" in R (v. 3.4.3; R Core Team, 2017). To contextualize the amount of embolism, we used freehand sections through the middles of the embolized tepals and visualized these sections using light microscopy to estimate the average number of vascular bundles, the average number of conduits per bundle, and the average conduit diameter. Conduit diameter was estimated as the average of two perpendicular cross sections of each conduit in 10–20 randomly selected vascular bundles per tepal. In May 2015, the experiment was repeated for *C. chinensis* and *C. occidentalis*, but there were too few scans of high enough quality to accurately characterize embolism in these species, so we restrict this analysis to *C. floridus*.

3 | RESULTS

3.1 | Climate variation

The two main measurement days in 2014 (May 5 and 11) differed in their atmospheric conditions (Figure 1). On May 5, temperature peaked at midday at 21 °C, whereas on May 11 temperature peaked in the early afternoon at 25 °C. These differences corresponded to different diurnal courses of VPD. On May 5, VPD peaked at 1.09 kPa, whereas on May 11, VPD peaked at 2.41 kPa.

3.2 | Pressure–volume relations

We used parameters calculated from water release curves and pressure–volume curves to characterize the drought responses of stems, leaves, and flowers (Figure 2). For all species, water potentials at turgor loss were higher for flowers than for leaves (Figure 2a), with significant effects of species (F = 16.28, p < .001), structure (F = 55.74, p < .001), and the interaction of species and structure (F = 4.13, p = .032). The differences between structures, however, were significant only for *C. occidentalis* (t = 6.65, p < .001) and *C. chinensis* (t = 6.87, p < .01). Comparisons of RWC_{TLP} were similar (Figure 2b), with a significant effect of species (F = 14.94, p < .001), structure (F = 22.98, p < .001), and the interaction of species and structure (F = 3.99, p = .034). The differences between structures were significant only for *C. occidentalis* (t = 3.69, p < .01) and *C. chinensis* (t = 7.77, p < .01). For all species, the saturated water content of flowers was higher than that of leaves (Figure 2c), with significant effects of species (F = 86.80, p < .001), structure (F = 1,095.61, p < .001), and the interaction between species and structure (F = 33.76, p < .001). Difference between structures were highly significant for all species (*C. floridus*: t = 14.30, *C. occidentalis*: t = 17.62, *C. chinensis*: t = 26.51; all p < .001). Mass-specific hydraulic capacitance differed similarly (Figure 2d), with higher capacitance in flowers than leaves and significant effects of species (F = 22.89, p < .001), structure (F = 194.40, p < .001), and the interaction of species and structure (F = 15.05, p < .001). Differences between leaves and flowers were significantly different for all species (*C. floridus*: t = 7.20, *C. occidentalis*: t = 9.44, *C. chinensis*: t = 6.43; all p < .001). Based on the regression of water released versus stem water potential, stems of *C. floridus* had higher mass-specific hydraulic capacitance than either *C. chinensis* or *C. occidentalis* (102.8, 100.7, 88.0 mol kg^{-1} MPa^{-1}, respectively), although this difference was not significant (p = .67), and stems of all species had higher hydraulic capacitance than either leaves or flowers (Figure 2d).

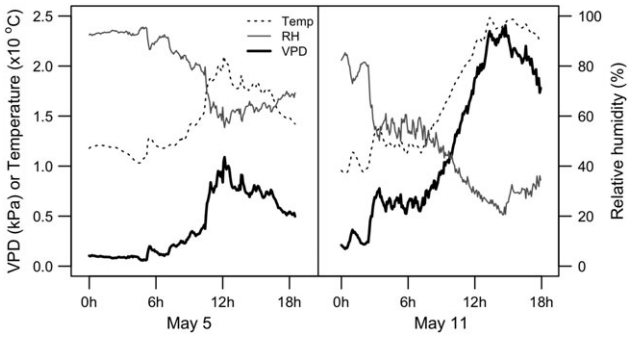

FIGURE 1 Diurnal variation in air temperature, relative humidity, and VPD during the two days of measurements. VPD = vapour pressure deficit; RH = relative humidity

3.3 | Diurnal variation in water status and gas exchange

Diurnal variation in gas exchange and water potential revealed differences between leaves and flowers. On May 5, 2014, measurements were made starting at predawn and continuing every 3 hr until 17:30 for *C. occidentalis* (Figure 3) and at predawn and midday for *C. chinensis*. Stomatal conductance and transpiration increased for both leaves and flowers throughout the day and peaked for both structures at 14:30. At this time, $g_{s,leaf}$ averaged 120 mmol m^{-2} s^{-1} and $g_{s,flower}$ averaged 90 mmol m^{-2} s^{-1}. Similarly, transpiration peaked at 14:30, averaging 1.26 and 0.81 mmol m^{-2} s^{-1} for leaves and flowers, respectively. At each time point, gas exchange rates were higher for leaves than they were for flowers (Figure 3a,b). Similarly, leaf water potentials at each measurement period were always lower than both stem and flower water potentials (Figure 3c) with midday minimum water potentials of −0.93 and − 0.77 MPa for leaves and flowers, respectively. The difference between stem and flower water potentials ($\Delta\Psi_{stem-flower}$) varied little during the days, peaking at only 0.10 MPa at 14:30, in contrast to $\Delta\Psi_{stem-leaf}$ which increased from 0.10 MPa at predawn to 0.25 MPa at midday. Measurements of water potential in May 2015 and 2016 showed similar patterns as measurements in 2014 for all three species (data for *C. floridus* in Figure S2). As a result of high E relative to the low $\Delta\Psi$, K_{flower} was higher than K_{leaf} at

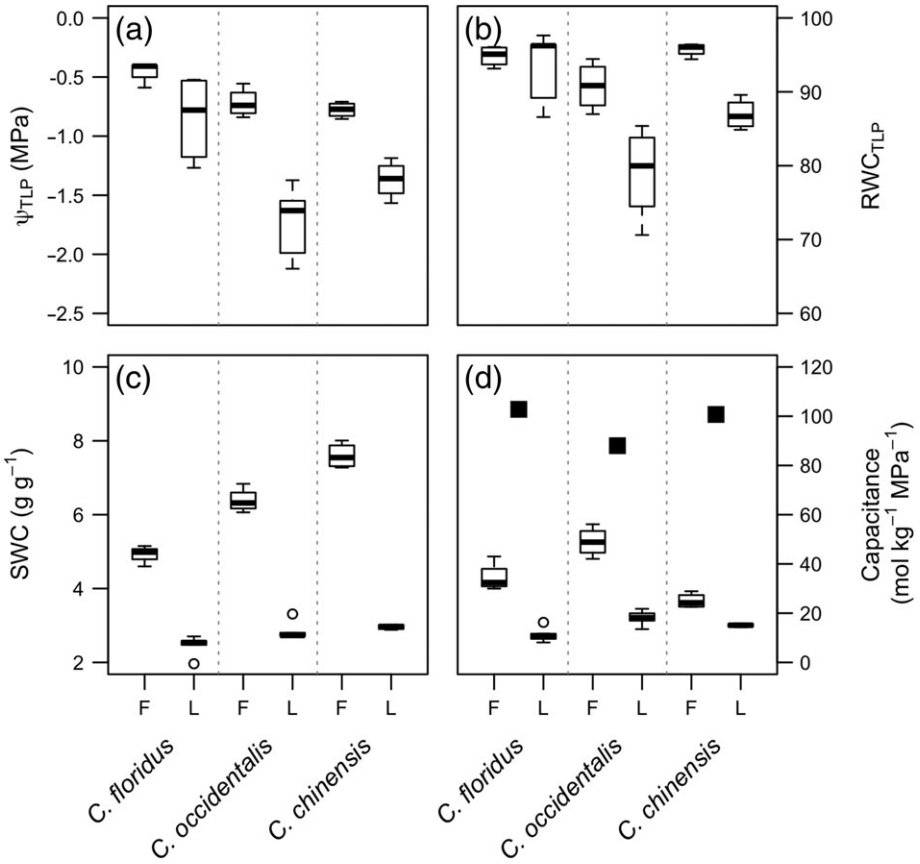

FIGURE 2 Parameters derived from the pressure–volume relationship for leaves (L) and flowers (F) of the three *Calycanthus* species: (a) water potential at the point of turgor loss, (b) relative water content at the point of turgor loss, (c) saturated water content relative to tissue dry mass, (d) hydraulic capacitance expressed as moles of water per kg dry mass per MPa. For comparison, stem capacitance values are plotted as filled squares in (d). RWC = relative water content; SWC = saturated water content

each time point except the last (Figure 3d). In the early afternoon (14:30), when E was highest, K_{flower} averaged 14.45 mmol m^{-2} s^{-1} MPa^{-1} whereas K_{leaf} averaged 5.04 mmol m^{-2} s^{-1} MPa^{-1}. These measurements of K_{flower} based on transpiration rate were lower than maximum K_{flower} determined in an earlier study using the vacuum pump method, except for the peak measurements of K_{flower} measured at midday (18.79 mmol m^{-2} s^{-1} MPa^{-1}, solid, horizontal line, and shading in Figure 3d; Roddy et al., 2016). In contrast, K_{leaf} increased throughout the day, peaking in the early evening (17:30) at 10.24 mmol m^{-2} s^{-1} MPa^{-1} despite declines in both $g_{s,leaf}$ and E_{leaf} after midday.

Because g_s and E peaked for both leaves and flowers at 14:30, on May 11, 2014, we subsequently measured gas exchange and water potentials at only this time and predawn for both *C. occidentalis* and *C. chinensis* (Figure 4). At predawn and midday, $g_{s,flower}$ was higher than $g_{s,leaf}$ for both species. Similar to measurements on May 5, Ψ_{flower} tracked changes in Ψ_{stem} throughout the day, such that $\Delta\Psi_{stem-flower}$ increased only slightly for *C. occidentalis*. In contrast, $\Delta\Psi$ increased much more from predawn to midday for *C. occidentalis* leaves and for leaves and flowers of *C. chinensis* (Figure 4c). Consequently, K_{flower} increased more than threefold for *C. occidentalis* but slightly decreased for *C. chinensis*. On this day, too, K_{flower} sometimes exceeded the average maximum value for flowers measured using the vacuum pump method for *C. occidentalis* flowers but not for *C. chinensis* (Figure 4d). K_{leaf} increased throughout the day for *C. occidentalis* but even at midday was less than one-third the value of K_{flower} for this species. K_{leaf} changed little throughout the day for *C. chinensis* (Figure 4d). Pressure–volume relationships had significant effects on these diurnal patterns of water potential, as maintaining a higher hydraulic capacitance significantly reduced midday $\Delta\Psi$ (R^2 = 0.69, p = .04; Figure 5).

Average water loss rates differed significantly among species (F = 10.48, p < .01) and structures (F = 62.69, p < .001). Flowers lost water more rapidly than leaves, and both leaves and flowers of *C. occidentalis* (0.23 mmol m^{-2} s^{-1} and 1.14 mmol m^{-2} s^{-1}, respectively) had higher water loss rates than those of *C. chinensis* (0.71 mmol m^{-2} s^{-1} and 0.10 mmol m^{-2} s^{-1}). As a result, there was a significant interaction between species and structure (F = 7.87, p < .01).

3.4 | Response of stomatal conductance to vapour pressure

We characterized the gas exchange responses to VPD of leaves and flowers of *C. occidentalis* (Figure 6). There was no significant difference between maximum g_s of leaves and tepals (120.8 ± 3.12 mmol m^{-2} s^{-1} and 152.8 ± 30.72 mmol m^{-2} s^{-1}, respectively; F = 1.075, p = .35). However, the VPD at 50% of maximum g_s differed among leaves and flowers. Tepal g_s was 50% of maximum at 1.41 kPa, whereas leaf g_s was 50% of maximum at 2.2 kPa.

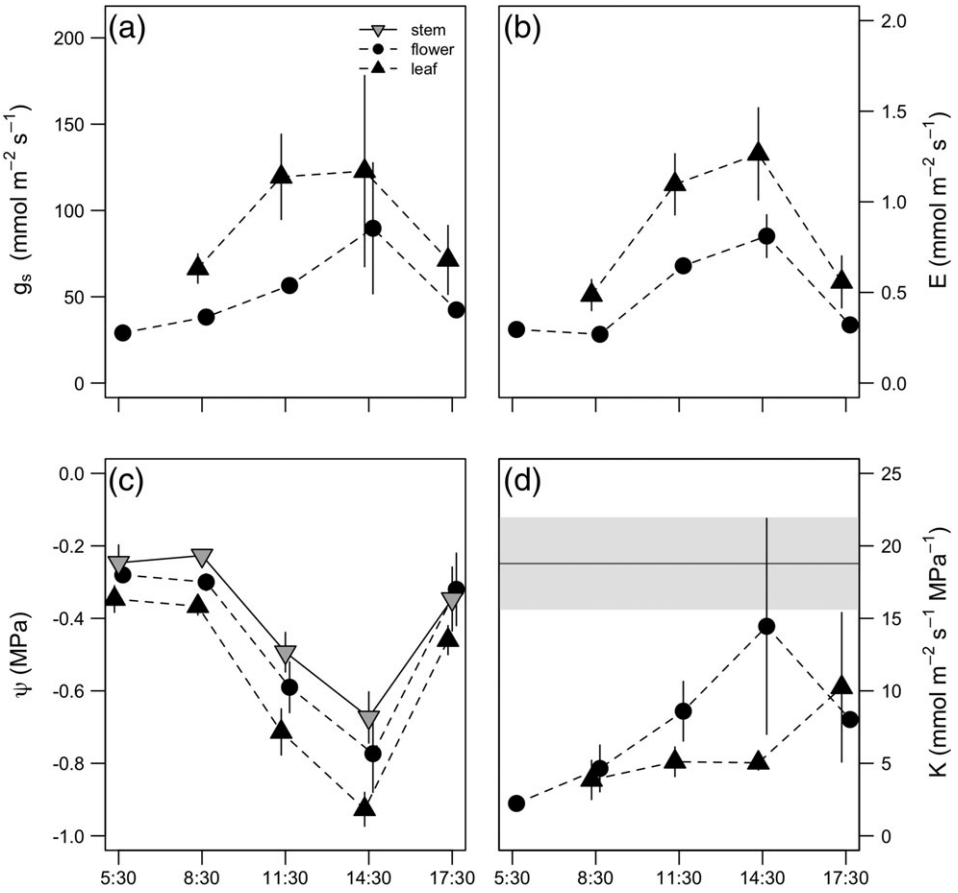

FIGURE 3 Diurnal measurements of (a) stomatal conductance, (b) transpiration, (c) water potential, and (d) hydraulic conductance on May 5 for *Calycanthus occidentalis*. Error bars represent standard error. Slight jitter in the horizontal axis has been added so that points and error bars do not overlap. In (d), the horizontal line and shading represent the average and standard error, respectively, of maximum K_{flower} for *Calycanthus occidentalis* reported in Roddy et al. (2016)

3.5 | Diurnal variation in water residence times

Flower water content (*W*) and residence times (τ) varied throughout the day, with τ varying substantially more than *W* (Figure 7). The large diurnal variation in τ (from approximately 30 hr predawn to approximately 12 hr at midday for *C. occidentalis* flowers on May 5) was driven predominantly by changes in *E* (Figure 3b) and not by changes in *W*. Although leaf τ varied diurnally in a similar pattern, this variation was less dramatic. On May 11, during which VPD was higher both predawn and throughout the day (Figure 1), predawn τ of flowers and leaves was higher than on May 5 (40–60 hr compared to 30 hr) but declined to similar values at midday, with little difference in midday τ between leaves and flowers of each species.

3.6 | Vulnerability to embolism in tepals

In the microCT experiment, water potentials of *C. floridus* ranged from −0.59 to −3.01 MPa, with no embolisms appearing until −2.03 MPa (Figures 8 and 9). In this range of water potentials, tepals had lost turgor and wilted and there was little intercellular air space still present. The water potential at 50% probability of embolism was estimated to be −2.30 ± 0.22 MPa, significantly lower than the turgor loss point for *C. floridus* tepals (−0.45 ± 0.05 MPa). There were 28 ± 0.67 vascular bundles per tepal and 6.19 ± 0.46 conduits per bundle (Figure S3). By rough approximation, then, there were approximately 173 conduits in cross section at the middle of the tepal. Interestingly, even at −3.01 MPa, only six conduits in total were embolized in the two tepals in this scan, suggesting that the vast majority of conduits were even more resistant to embolism formation. The diameters of embolized conduits (8.97 ± 0.75 μm) were slightly larger than the entire population of conduits in the samples (7.45 ± 0.38 μm), but this difference was not significant.

4 | DISCUSSION

Many species flower under physiologically stressful conditions, such as when water is limiting. Yet maintaining flower function—turgid floral displays and receptivity—despite these resource demands is critical for sexual reproduction in many species. Even species native to mesic habitats, such as the *Calycanthus* species studied here, must support their flowers when atmospheric demand for water is high. Despite being well-watered, having high hydraulic capacitance (Figure 2) and having high K_{flower} (Figures 3 and 4; Roddy et al., 2016), *C. occidentalis* flowers visibly wilted by midday when VPD was high. This suggests that *Calycanthus* flowers—and, perhaps, flowers more generally—may function near the limits of their physiological capacities.

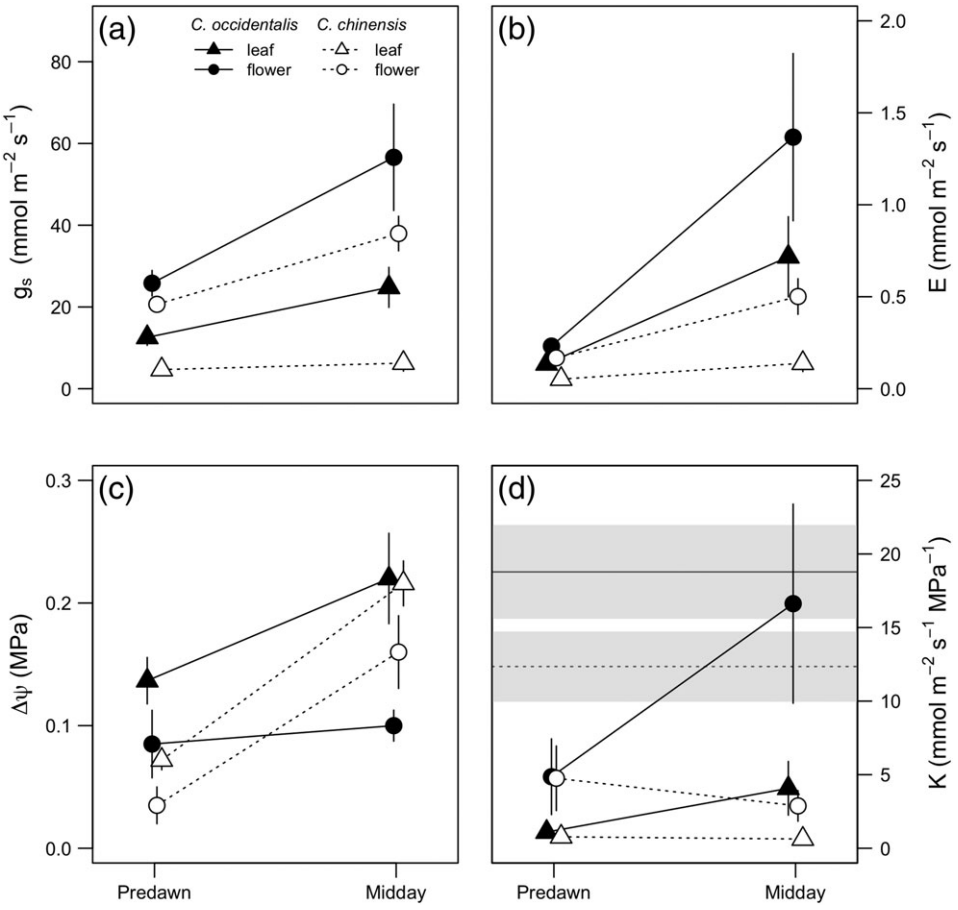

FIGURE 4 Predawn and midday measurements of (a) stomatal conductance, (b) transpiration, (c) water potential gradients between stems and either leaves or flowers, and (d) hydraulic conductance of leaves and flowers for two *Calycanthus* species on May 11. In (d), the horizontal lines and shading represent the averages and standard errors, respectively, of maximum K_{flower} for *Calycanthus occidentalis* (solid) and *Calycanthus chinensis* (dotted) from Roddy et al. (2016)

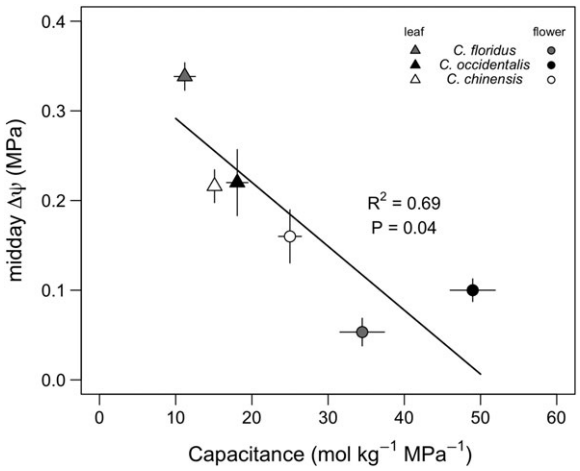

FIGURE 5 Trade-off between hydraulic capacitance and midday water potential gradients ($\Delta\Psi_{stem-leaf}$ or $\Delta\Psi_{stem-flower}$) pooled across species and days

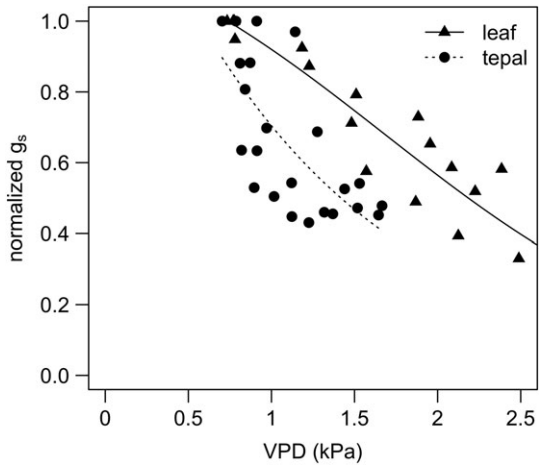

FIGURE 6 The responses of stomatal conductance for leaves and tepals of *Calycanthus occidentalis* to the vapour pressure deficit driving transpiration. For each replicate, measurements of stomatal conductance were normalized to the maximum measured g_s

4.1 | Function of the xylem hydraulic pathway in flowers

Flowers of all three *Calycanthus* species exhibited water potentials indicative of a functional xylem hydraulic pathway. First, flower water potentials varied diurnally, tracking the water potentials of stems and leaves. Some have argued based on differences between leaf and flower water potentials that flowers may be hydrated by the phloem

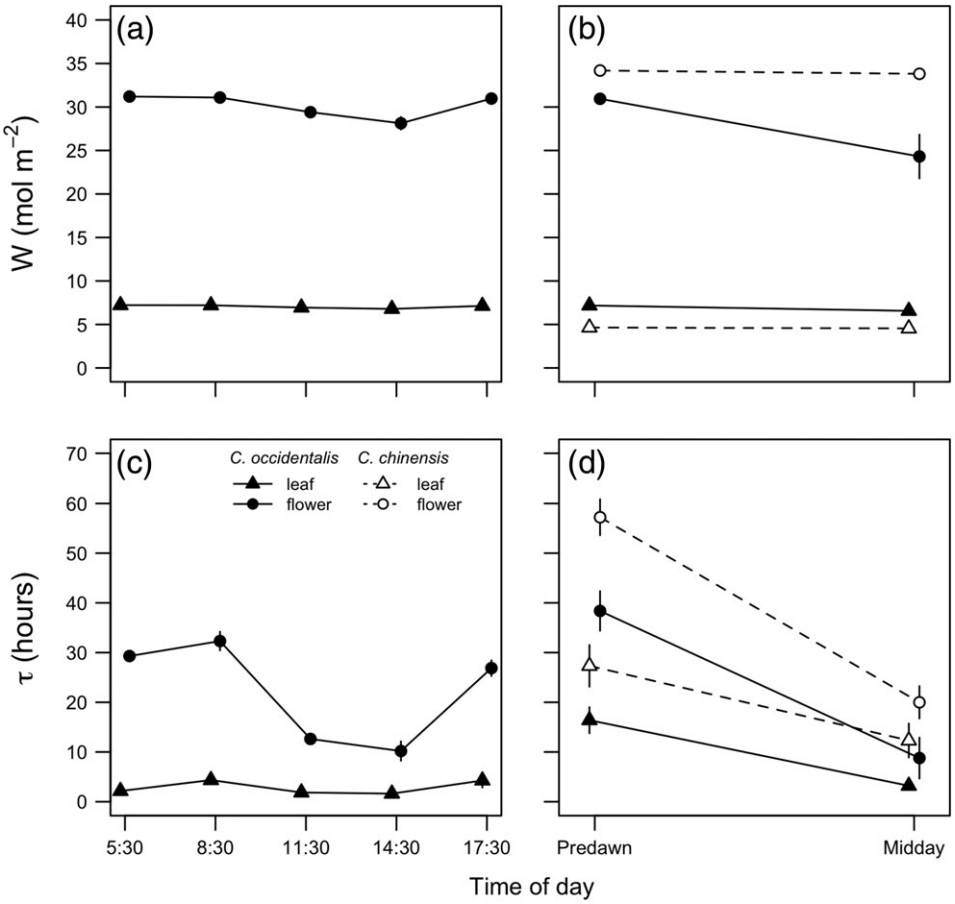

FIGURE 7 Diurnal variation in (a, b) water content (W) and (c, d) water residence times (τ) calculated from diurnal measurements of gas exchange and water potential measured (a, c) on May 5, 2014 and (b, d) on May 11, 2014 and from pressure–volume curve parameters (Figure S1) for *Calycanthus occidentalis* and *Calycanthus chinensis* leaves and flowers. Points and vertical lines represent means and standard error

rather than the xylem (Chapotin et al., 2003). Here, however, our data for *Calycanthus* flowers agree with those from *Illicium anisatum* and *Magnolia grandiflora* that suggest that flowers are connected to the stem xylem during anthesis because Ψ_{flower} was intermediate between Ψ_{stem} and Ψ_{leaf} (Figures 3, 4, and S2; Feild et al., 2009a, 2009b). Published data unequivocally showing the reverse Ψ gradients between stems and flowers thought to be indicative of phloem-hydration of flowers have been reported only for inner whorl tepals of *Magnolia grandiflora* (Feild et al., 2009b).

Second, occlusion of the xylem (Knipfer et al., 2015) and xylem discontinuity in the flower receptacle (Lersten & Wemple, 1966) could provide the spatial precision needed to differentially isolate heterotrophic and autotrophic floral structures (e.g., the calyx and corolla) and to generate the large water potential gradients observed between them (Trolinder et al., 1993). In *Calycanthus*, however, we found no evidence of xylem occlusion or discontinuity in the xylem pathway to the flower, particularly given the high values of K_{flower} in the genus and those measured diurnally here (Figures 3 and 4; Roddy et al., 2016). Like other magnoliid flowers, *Calycanthus* lacks a distinct calyx and corolla. It may be that the evolution of a perianth differentiated into distinct autotrophic and heterotrophic structures also involved physiological differentiation in the mechanisms used to maintain water balance.

More studies characterizing the function of the xylem hydraulic pathway throughout development and the relative importance of xylem versus phloem flow for flowers is needed and could change our perspective on how flowers are hydrated, similar to research on fruits (e.g., Choat, Gambetta, Shackel, & Matthews, 2009; Higuchi & Sakuratani, 2006; Johnson, Dixon, & Lee, 1992; Windt, Gerkema, & Van As, 2009).

4.2 | Hydraulic capacitance buffers flower water dynamics

Despite the connection to stem water supply, *Calycanthus* flowers also exhibited high hydraulic capacitance (Figure 2), which modulated variation in other physiological traits. A large storage reservoir can discharge substantial amounts of water for very small changes in water content, helping to prevent declines in water potential. Indeed, across all species and structures, high hydraulic capacitance mitigated the gradient between Ψ_{stem} and either Ψ_{leaf} or Ψ_{flower} (Figure 5). As a result, high hydraulic capacitance helped flowers delay reaching their turgor loss points and wilting.

The high water contents and absolute hydraulic capacitances of *Calycanthus* flowers further facilitated lengthy water turnover times that compensated for high transpiration rates from *C. occidentalis* and *C. chinensis* flowers (Figures 2–4). Gas exchange rates measured here for *C. occidentalis* and *C. chinensis* flowers were among the highest rates measured on flowers. Only tepals of avocado (*Persea*

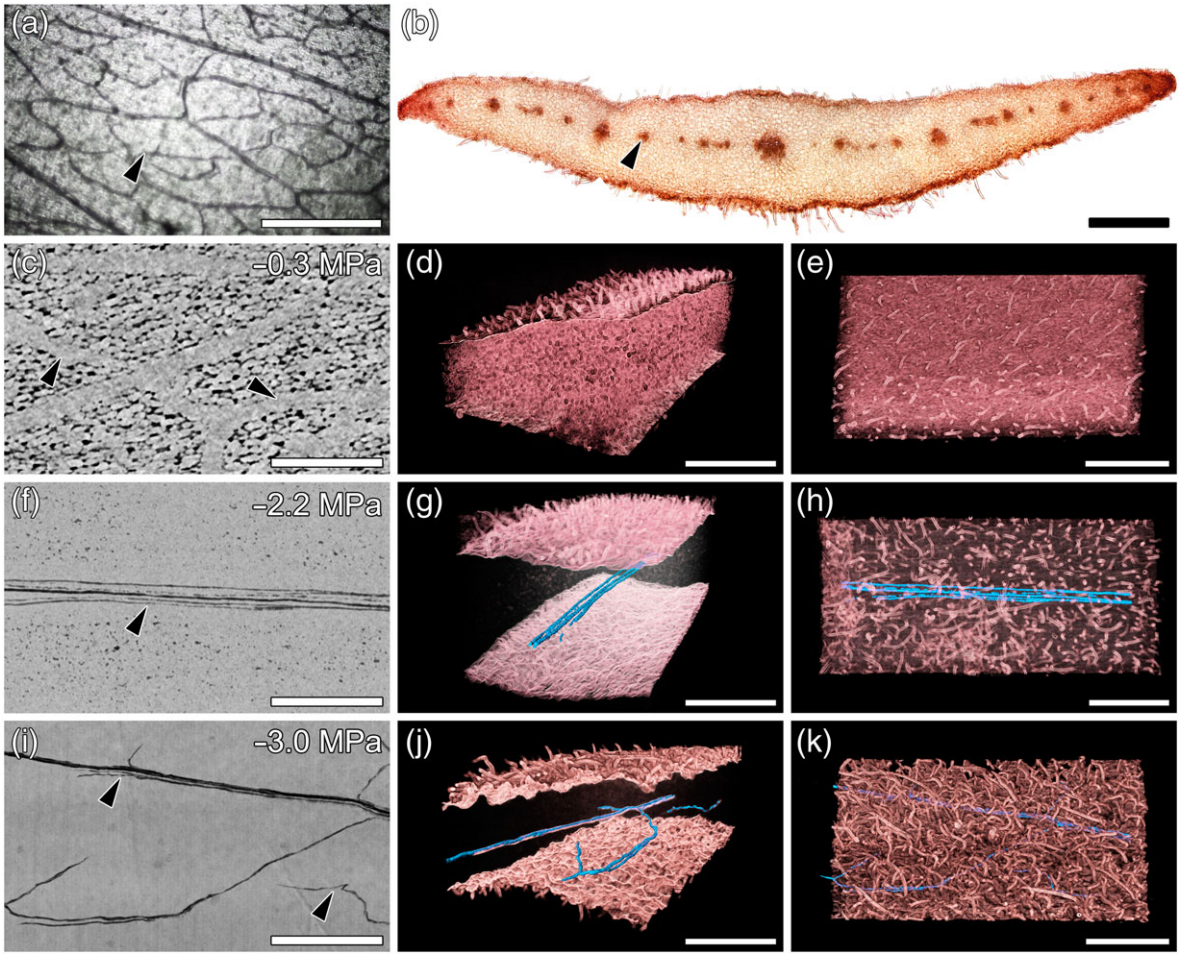

FIGURE 8 Vascular arrangement and embolism formation in *Calycanthus floridus* tepals. (a, b) Representative light microscopy images of (a) a paradermal section showing vein density and (b) a cross section of a tepal showing vascular bundle arrangement (black arrows). Two-dimensional and three-dimensional microCT images in different orientations showing representative tepals (c–e) prior to turgor loss (−0.3 MPa), (f–h) after turgor loss with embolism apparent only in a lateral vein (black arrow; −2.2 MPa), and (i–k) at −3.0 MPa with embolism in multiple vein orders. (c, f, i) Two-dimensional paradermal slices where black indicates air and grey indicates hydrated tissue. (c) Black arrows point to veins which are not embolized, and black regions show intercellular airspace. (f, i) Arrows point to embolized conduits (black) surrounded by hydrated cells (grey). Three-dimensional volume renderings of tepals in (d, g, j) oblique and (e, h, k) paradermal views. Renderings were optimized to highlight air–water interfaces, which appear red in colour. Regions with little air appear transparent. Embolized conduits in the samples at −2.2 and − 3.0 MPa (g, h, j, k) are highlighted in blue. Scale bars = 500 μm in all panels but varies with perspective in the microCT volume renderings

americana), another magnoliid, had transpiration rates comparable to those we measured for *Calycanthus* flowers (1.2–1.3 mmol m^{-2} s^{-1}; Blanke & Lovatt, 1993). Diurnal changes in *E* and g_s observed here are similar to diurnal changes measured in other magnoliid flowers (Feild et al., 2009b) but notably different from estimates of *E* measured in eudicot *Cistus* species, in which *E* increased linearly with VPD, as might be expected if floral stomata are non-functional (Hew, Lee, & Wong, 1980; Teixido & Valladares, 2014). In contrast to previous measurements (Feild et al., 2009b; Roddy & Dawson, 2012), E_{flower} of *C. occidentalis* and *C. chinensis* was higher than E_{leaf}, due to higher maximum g_s (Figures 3 and 4). However, data from *C. occidentalis* showed that tepal g_s was more sensitive to VPD than leaf g_s (Figure 6). This greater sensitivity of tepal g_s is probably due, in part, to the significantly higher Ψ_{TLP} of flowers (Figure 2a). Interestingly, such high g_s occurred in *C. occidentalis* tepals despite their having a stomatal density of only 14.31 mm^{-2}, suggesting that the high cuticular conductances of *Calycanthus* flowers, which are the highest among any flowers measured (Roddy et al., 2016), make significant contributions to total *E*. Consistent with high cuticular conductance, g_s reached its minimum and plateaued at 50% of maximum g_s between approximately 1–1.5 kPa (Figure 6). This suggests that approximately half of maximum measured g_s in *C. occidentalis* is due to cuticular conductance. Such high rates of water loss across the cuticle would allow flowers to have a high *E* to maintain floral temperatures below a critical, perhaps damaging, threshold temperature (Patiño et al., 2002; Patiño & Grace, 2002) and provide curious beetles with a cool environment, thereby facilitating pollination (Grant, 1950). Thus, high *W* and capacitance in flowers would ensure that there is sufficient water to maintain the high cuticular conductance that may be needed to maintain a cool flower and remain attractive to pollinators.

For *C. occidentalis* and *C. chinensis* flowers, *W* varied relatively little throughout the day when Ψ_{flower} was higher than Ψ_{TLP}, but still more than leaf *W* varied, reflecting the greater reliance on stored

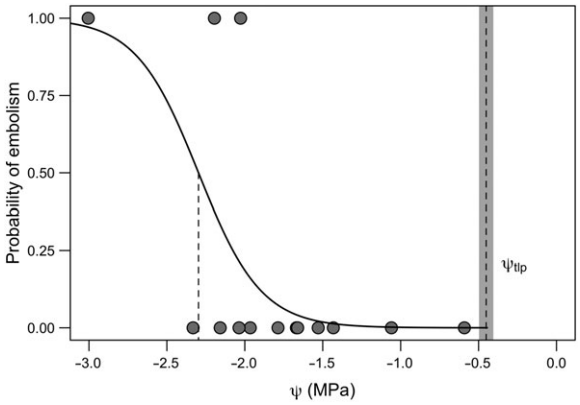

FIGURE 9 Probability of having any embolized conduits of *Calycanthus floridus* tepals as assessed by microCT imaging. The curve fit is indicated by a solid line with the water potential at 50% probability of embolism indicated by a dashed vertical line (−2.30 ± 0.22 MPa). The mean ± *SE* turgor loss point is indicated by the vertical dashed line and shading. At −3.01 MPa only six conduits were embolized

water to supply transpiration in flowers (Figure 7). Thus, prior to turgor loss, variation in τ was driven predominantly by variation in *E*. However, the large declines in *W* after turgor loss (Figure S1) brought midday τ close to that of conspecific leaves (Figure 7d). τ of *C. occidentalis* flowers ranged from approximately 12–40 hr; assuming these flowers live for 3 days, their water would turnover only two to six times. In contrast, *C. occidentalis* leaf water would turnover more than 10 times in the same period.

High hydraulic capacitance, therefore, slows down the rate of change in Ψ_{flower} and lengthens τ. If the diurnal rate of change in abiotic conditions and Ψ_{stem} is sufficiently fast, then maintaining a high hydraulic capacitance may be an effective strategy of preventing turgor loss, thus compensating for flowers having a high Ψ_{TLP}. In flowers or fruits with long lifespans, water stored in these structures may even flow back to the stem, such as has been shown for developing mango fruits (Higuchi & Sakuratani, 2006).

Hydraulic capacitance would also help prevent embolism formation and spread, potentially extending floral lifespan. In *C. floridus* flowers, there was no embolism until −2.03 MPa, similar to data from four eudicot flowers (Zhang & Brodribb, 2017), and even at −3.01 MPa less than 4% of conduits were embolized (Figures 8 and 9). These results indicate that *C. floridus* flowers have a large safety margin (approximately 1.85 MPa) between turgor loss and embolism formation (Figure 9), suggesting that even if flowers lose turgor diurnally (as *C. occidentalis* flowers did), they may not suffer embolism. Autotrophic structures such as leaves must certainly avoid embolism to remain functional, but the effects of embolism formation on heterotrophic structures such as flowers is unclear. Maintaining a functional xylem pathway in showy corollas may matter little as long as it does not impede their ability to attract pollinators and supply growing embryos.

5 | CONCLUSIONS

Despite the importance of flowers to reproduction, relatively little is known about their physiology and water relations. Here, we show that *Calycanthus* flowers can have high stomatal and cuticular conductances and transpiration, sometimes exceeding those of subtending leaves. *Calycanthus* flowers are unique in having among the highest hydraulic conductances of any flowers measured, and whereas flower stomata are more sensitive to VPD than foliar stomata, a high cuticular conductance means that transpiration remains high even after stomatal closure, magnifying the water resource costs associated with flower production and maintenance. Despite relying on the xylem for water delivery, *Calycanthus* flowers are very resistant to embolism formation and spread, perhaps because of high hydraulic capacitance, which lengthens water turnover times, maintains high water potentials, and may delay turgor loss. However, under even moderate increases in air temperature and VPD, these flowers regularly wilt by midday, suggesting that they may function on the edge of their physiological capacities. These complex interactions between different physiological strategies could have important consequences for floral function under changing climates and for our understanding of the evolution of flower form and function.

ACKNOWLEDGMENTS

The authors thank H.F. for providing access to plants at the U.C. Botanical Garden and D.P. and A.M. for their assistance at the Lawrence Berkeley National Laboratory Advanced Light Source Beamline 8.3.2 microtomography facility. The Advanced Light Source is supported by the Director, Office of Science, Office of Basic Energy Services, of the U.S. Department of Energy under contract no. DE-AC01-05CH11231. F.M. and two reviewers provided critical and productive feedback on a previous draft. A.B.R. was supported by a Graduate Research Fellowship from the U.S. National Science Foundation and by research support from the Yale Institute for Biospheric Studies.

ORCID

Adam B. Roddy http://orcid.org/0000-0002-4423-8729
Craig R. Brodersen http://orcid.org/0000-0002-0924-2570

REFERENCES

Bazzaz, F. A., Chiariello, N. R., Coley, P., & Pitelka, L. F. (1987). Allocating resources to reproduction and defense. *Bio Science*, *37*, 58–67.

Blanke, M. M., & Lovatt, C. J. (1993). Anatomy and transpiration of the avocado inflorescence. *Annals of Botany*, *71*, 543–547.

Brodersen, C. R., & Roddy, A. B. (2016). New frontiers in the three-dimensional visualization of plant structure and function. *American Journal of Botany*, *103*, 184–188.

Brodribb, T. J., Holbrook, N. M., Zwieniecki, M. A., & Palma, B. (2005). Leaf hydraulic capacity in ferns, conifers and angiosperms: Impacts on photosynthetic maxima. *New Phytologist*, *165*, 839–846.

Brown, R. W., & Bartos, D. L. (1982). *A calibration model for screen-caged Peltier thermocouple psychrometers*. Ogden, Utah: Intermountain Forest and Range Experiment Station, United States Department of Agriculture.

Buck, A. (1981). New equations for computing vapor pressure and enhancement factor. *Journal of Applied Meteorology*, *20*, 1527–1532.

Chapotin, S. M., Holbrook, N. M., Morse, S., & Gutiérrez, M. V. (2003). Water relations of tropical dry forest flowers: Pathways for water entry

and the role of extracellular polysaccharides. *Plant, Cell & Environment*, *26*, 623–630.

Choat, B., Gambetta, G. A., Shackel, K. A., & Matthews, M. A. (2009). Vascular function in grape berries across development and its relevance to apparent hydraulic isolation. *Plant Physiology*, *151*, 1677–1687.

De la Barrera, E., & Nobel, P. S. (2004). Nectar: Properties, floral aspects, and speculations on origin. *Trends in Plant Science*, *9*, 65–69.

Feild, T. S., Chatelet, D. S., & Brodribb, T. J. (2009a). Ancestral xerophobia: A hypothesis on the whole plant ecophysiology of early angiosperms. *Geobiology*, *7*, 237–264.

Feild, T. S., Chatelet, D. S., & Brodribb, T. J. (2009b). Giant flowers of southern magnolia are hydrated by the xylem. *Plant Physiology*, *150*, 1587–1597.

Fenster, C. B., Armbruster, W. S., Wilson, P., Dudash, M. R., & Thomson, J. D. (2004). Pollination syndromes and floral specialization. *Annual Review of Ecology, Evolution, and Systematics*, *35*, 375–403.

Galen, C. (1999). Why do flowers vary? *Bio Science*, *49*, 631–640.

Galen, C., Dawson, T. E., & Stanton, M. L. (1993). Carpels and leaves: Meeting the carbon cost of reproduction in an alpine buttercup. *Oecologia*, *95*, 187–193.

Galen, C., Sherry, R. A., & Carroll, A. B. (1999). Are flowers physiological sinks or faucets? Costs and correlates of water use by flowers of *Polemonium viscosum*. *Oecologia*, *118*, 461–470.

Grant, V. (1950). The pollination of *Calycanthus occidentalis*. *American Journal of Botany*, *37*, 294–297.

Herrera, C. (1996). In D. Lloyd, & S. Barrett (Eds.), *Floral traits and plant adaptation to insect pollinators: A devil's advocate approach* (pp. 65–87). New York: Chapman & Hall.

Hew, C. S., Lee, G. L., & Wong, S. C. (1980). Occurrence of non-functional stomata in the flowers of tropical orchids. *Annals of Botany*, *46*, 195–201.

Higuchi, H., & Sakuratani, T. (2006). Dynamics in mango (*Mangifera indica* L.) fruit during the young and mature fruit seasons as measured by the stem heat balance method. *Journal of the Japanese Society for Horticultural Science*, *75*, 11–19.

Johnson, R. W., Dixon, M. A., & Lee, D. R. (1992). Water relations of the tomato during fruit growth. *Plant, Cell and Environment*, *15*, 947–953.

Knipfer, T., Fei, J., Gambetta, G. A., McElrone, A. J., Shackel, K. A., & Matthews, M. A. (2015). Water transport properties of the grape pedicel during fruit development: Insights into xylem anatomy and function using microtomography. *Plant Physiology*, *168*, 1590–1602.

Lambrecht, S. C. (2013). Floral water costs and size variation in the highly selfing *Leptosiphon bicolor* (Polemoniaceae). *International Journal of Plant Sciences*, *174*, 74–84.

Lambrecht, S. C., & Dawson, T. E. (2007). Correlated variation of floral and leaf traits along a moisture availability gradient. *Oecologia*, *151*, 574–583.

Lersten, N. R., & Wemple, D. K. (1966). The discontinuity plate, a definitive floral characteristic of the Psoraleae (Leguminosae). *American Journal of Botany*, *53*, 548–555.

McCulloh, K. A., Johnson, D. M., Meinzer, F., & Woodruff, D. (2014). The dynamic pipeline: Hydraulic capacitance and xylem hydraulic safety in four tall conifer species. *Plant, Cell & Environment*, *37*, 1171–1183.

Meinzer, F., James, S. A., Goldstein, G., & Woodruff, D. (2003). Whole-tree water transport scales with sapwood capacitance in tropical forest canopy trees. *Plant, Cell & Environment*, *26*, 1147–1155.

Meinzer, F. C., Johnson, D. M., Lachenbruch, B., McCulloh, K. A., & Woodruff, D. R. (2009). Xylem hydraulic safety margins in woody plants: Coordination of stomatal control of xylem tension with hydraulic capacitance. *Functional Ecology*, *23*, 922–930.

Meinzer, F. C., Woodruff, D. R., Domec, J.-C., Goldstein, G., Campanello, P. I., Gatti, M. G., & Villalobos-Vega, R. (2008). Coordination of leaf and stem water transport properties in tropical forest trees. *Oecologia*, *156*, 31–41.

Patiño, S., & Grace, J. (2002). The cooling of convolvulaceous flowers in a tropical environment. *Plant, Cell & Environment*, *25*, 41–51.

Patiño, S., Jeffree, C., & Grace, J. (2002). The ecological role of orientation in tropical convolvulaceous flowers. *Oecologia*, *130*, 373–379.

R Core Team (2017). *R: A language and environment for statistical computing*. Vienna, Austria: R Foundation for Statistical Computing.

Reekie, E. G., & Bazzaz, F. A. (1987a). Reproductive effort in plants. 2. Does carbon reflect the allocation of other resources? *The American Naturalist*, *129*, 897–906.

Reekie, E. G., & Bazzaz, F. A. (1987b). Reproductive effort in plants. 1. Carbon allocation to reproduction. *The American Naturalist*, *129*, 876–896.

Roddy, A. B., Brodersen, C. R., & Dawson, T. E. (2016). Hydraulic conductance and the maintenance of water balance in flowers. *Plant, Cell & Environment*, *39*, 2123–2132.

Roddy, A. B., & Dawson, T. E. (2012). Determining the water dynamics of flowering using miniature sap flow sensors. *Acta Horticulturae*, (951), 47–54.

Roddy, A. B., Guilliams, C. M., Lilittham, T., Farmer, J., Wormser, V., Pham, T., … Dawson, T. E. (2013). Uncorrelated evolution of leaf and petal venation patterns across the angiosperm phylogeny. *Journal of Experimental Botany*, *64*, 4081–4088.

Ruedin, C. T., Schindelin, J., Hiner, M. C., DeZonia, B. E., Walter, A. E., Arena, E. T., & Eliceri, K. W. (2017). Image J2: Image J for the next generation of scientific image data. *BMC Bioinformatics*, *18*, 529.

Simonin, K. A., & Roddy, A. B. (2018). Genome downsizing, physiological novelty, and the global dominance of flowering plants. *PLoS Biology*, *16*, e2003706.

Specht, C. D., & Bartlett, M. E. (2009). Flower evolution: The origin and subsequent diversification of the angiosperm flower. *Annual Review of Ecology, Evolution, and Systematics*, *40*, 217–243.

Sprengel, C. (1793). *Das entdeckte Geheimniss der Natur im Bau und in der Befruchtung der Blumen*. Berlin: Friedrich Vieweg dem Aeltern.

Sprengel, C. (1996). In D. Lloyd, & S. Barrett (Eds.), *Discovery of the secret nature in the structure and fertilization of flowers* (pp. 3–43). New York, NY: Chapman & Hall.

Strauss, S., & Whittall, J. (2006). *Non-pollinator agents of selection on floral traits*. (pp. 120–138). New York: Oxford University Press.

Teixido, A. L., & Valladares, F. (2013). Large and abundant flowers increase indirect costs of corollas: A study of coflowering sympatric Mediterranean species of contrasting flower size. *Oecologia*, *173*, 73–81.

Teixido, A. L., & Valladares, F. (2014). Disproportionate carbon and water maintenance costs of large corollas in hot Mediterranean ecosystems. *Perspectives in Plant Ecology, Evolution and Systematics*, *16*, 83–92.

Trolinder, N., McMichael, B., & Upchurch, D. (1993). Water relations of cotton flower petals and fruit. *Plant, Cell & Environment*, *16*, 755–760.

Tyree, M. T., & Hammel, H. T. (1972). The measurements of the turgor pressure and the water relations of plants by the pressure-bomb technique. *Journal of Experimental Botany*, *23*, 267–282.

Whitehead, D. (1998). Regulation of stomatal conductance and transpiration in forest canopies. *Tree Physiology*, *18*, 633–644.

Windt, C. W., Gerkema, E., & Van As, H. (2009). Most water in the tomato truss is imported through the xylem, not the phloem: A nuclear magnetic resonance flow imaging study. *Plant Physiology*, *151*, 830–842.

Zhang, F.-P., & Brodribb, T. J. (2017). Are flowers vulnerable to xylem cavitation during drought? *Proceedings of the Royal Society B: Biological Sciences*, *284*, 20162642.

Zhang, F.-P., Yang, Y.-J., Yang, Q.-Y., Zhang, W., Brodribb, T. J., Hao, G.-Y., … Zhang, S.-B. (2017). Floral mass per area and water maintenance traits are correlated with floral longevity in *Paphiopedilum* (Orchidaceae). *Frontiers in Plant Science*, *08*, 501.

Zhou, S., Renner, S. S., & Wen, J. (2006). Molecular phylogeny and intra- and intercontinental biogeography of Calycanthaceae. *Molecular Phylogenetics and Evolution*, *39*, 1–15.

SUPPORTING INFORMATION

Additional Supporting Information may be found online in the supporting information tab for this article.

How to cite this article: Roddy AB, Simonin KA, McCulloh KA, Brodersen CR, Dawson TE. Water relations of *Calycanthus* flowers: Hydraulic conductance, capacitance, and embolism resistance. *Plant Cell Environ*. 2018;41:2250–2262. https://doi.org/10.1111/pce.13205